Effects of Zinc Binding on the Conformational Distribution of the Amyloid-β Peptide Based on Molecular Dynamics Simulations

Wenfei Li, Jian Zhang, Yu Su, Jun Wang, Meng Qin, and Wei Wang*

National Laboratory of Solid State Microstructure and Department of Physics, Nanjing University, Nanjing 210093, China

Received: August 2, 2007

A number of experiments suggested that metal binding can promote the aggregation of the amyloid-β peptide. In this work, the effects of the zinc binding on the conformational distributions of the full length amyloid-β peptide are investigated on the basis of extensive molecular dynamics simulations. By comparing the conformational distributions of the apo-peptide and the holo-peptide, we show that the zinc binding can affect the conformational distribution of the amyloid-β monomer dramatically. Compared with the apo-peptide, the holo-peptide samples more β-strand conformation for the central hydrophobic cluster 17−21. Meanwhile, the formation probabilities of the salt bridge Asp23−Lys28 and the turn comprising 23−28 are also increased significantly at room temperature. Since these local structures are essential for the amyloid-β aggregation, the observed effects of the zinc binding indicate that the metal induced conformational change of the monomer is one of the possible mechanisms for the metal promoted aggregation of the amyloid-β peptide.

I. Introduction

Aggregation of the amyloid-β peptide (Aβ) is believed to be the main pathogeny of Alzheimer's disease (AD).[1,2] In aqueous solvent or a membrane-mimicking environment, the Aβ mainly adopts α helix and random coil conformations.[3−6] However, in fibrils, the secondary structures are dominated by parallel β sheet.[7] Therefore, during the aggregation of the Aβ peptide, the monomer undergoes conformational conversion from α helix or random coil to β strand. Since the conformations of the Aβ monomer in solution may influence such conformational transition, investigating the conformational distribution and the factors affecting it is fundamental for understanding the mechanisms of the Aβ aggregation and fibrillation.[8]

Accumulating evidence suggests that the metal binding can promote the protease resistent aggregation of the Aβ and the development of the AD.[9] For example, anatomy studies found that the concentrations of the Zn(II) and Cu(II) in the Aβ plaques of the AD patients are dramatically higher than the normal level.[10] Meanwhile, experiments found that the metal-induced aggregation of both the synthetic Aβ and the Aβ derived from human post-mortem brain specimens can be reversed by removing the metal ions with the metal ion chelators.[11] In addition, in vitro experiments observed that the Zn(II) can promote the aggregation of the Aβ within wide pH range.[12] The Cu(II) can also affect the aggregation of the Aβ at slightly acidic environments.[13,14] These results imply that the metal binding plays major roles in the Aβ aggregation and the development of the AD. Investigating the molecular mechanism of the metal induced aggregation and fibrillation of the Aβ peptide and the factors which can inhibit the pathogenic binding of the metal ions will be helpful for treating the related diseases.

In literature, two possible mechanisms for the metal induced aggregation of the Aβ peptide are proposed:[15−17] (I) the metal ion binds to two Aβ monomers simultaneously and promotes the aggregation by bridging the peptides, and (II) each metal ion binds to one monomer and results in conformational transition, which contributes to the Aβ aggregation. During the past decade, a number of experiments have been devoted to studying the metal induced conformational transition of the Aβ monomer and the amyloid fibril formation, and many valuable results have been obtained.[14−18] Most recently, the coordination mode of the Zn(II) to the Aβ peptide was identified on the basis of the nuclear magnetic resonance (NMR) spectrum of the Aβ segment.[18] It was found that the residues His6, His13, His14, and Glu11 are the ligands that tetrahedrally coordinate to the Zn(II). However, up to now, the effects of the metal binding on the conformational distribution and the conformational transition of the Aβ monomer are still unclear, requiring further experimental and theoretical investigations. Experimentally, as the Aβ peptide is prone to aggregate and difficult to crystallize, the structural characterizations of the Aβ monomer in aqueous solvent based on the regular NMR and X-ray diffraction techniques are hindered. Such limitations make the experimental investigations of the metal induced conformational transition and amyloid fibril formation much more difficult. Molecular dynamics (MD) simulations, because of its high temporal and spacial resolutions, are extensively employed in studying the conformational distribution and the structural transition of the full length Aβ and its shortened fragments.[8,19−27] In this work, we try to use the MD simulations to study the metal ion induced variation of the conformational distribution and the possible mechanisms of the metal promoted aggregation of the Aβ peptide.

By comparing the conformational distributions of the Aβ peptides with and without zinc binding, we show that the zinc binding can affect the conformational distribution of the Aβ monomer dramatically. Particularly, it is found that the zinc binding can increase the formation probabilities of the β-strand in the central hydrophobic cluster 17−21, the salt bridge Asp23-Lys28, and the turn comprising the residues 23−28. Since these local structures play important roles in the Aβ aggre-

* Corresponding author. E-mail: wangwei@nju.edu.cn.

10.1021/jp076213t CCC: $37.00 © 2007 American Chemical Society
Published on Web 11/15/2007

gation,[19,23,28−35] the enhancements of these local structures by the zinc binding indicate that the zinc binding can contribute to the Aβ pathogenic folding and amyloid fibril formation. Our results suggest that the metal induced conformational variation of the Aβ monomer is one of the possible mechanisms for the metal promoted aggregation of the Aβ peptide.

II. Model and Methods

A. Replica Exchange Molecular Dynamics Model. Replica exchange method is a high efficiency sampling technique which was first implemented in molecular dynamics model by Sugita and Okamoto[36] and was widely used in the studying of protein folding and aggregation.[37−45] In replica exchange molecular dynamics (REMD) simulations, N non-interacting replicas at N different temperatures are conducted simultaneously in parallel. After a certain MD step, the exchange of replica between neighbor temperatures are attempted. The acceptance ratio of exchange is determined by the energy difference and temperature difference between the replica pair with Metropolis criterion:

$$P(X_i \rightarrow X_j) = \min(1, \exp(-\Delta)) \quad (1)$$

where $\Delta = (\beta_i - \beta_j)(E_j - E_i)$ with β and E being the invert temperature and potential energy, respectively. With this method, the configurations at low temperatures have ability to overcome high-energy barriers by being switched to high temperatures, and it provides improved sampling at lower temperatures than standard MD.

B. Simulation Details. In this work, the simulations are performed employing the AMBER8 molecular dynamics simulation package with the standard ff03 force field being used.[46,47] In treating the solvent effects, the generalized Born (GB) model is used.[48] With the implicit treatment of the solvent effects, the simulation can be well-converged within reasonable simulation time. We conducted two REMD simulations, that is, simulations with zinc binding (holo-peptide) and without zinc binding (apo-peptide). Both the simulations are started from random conformations.

For the simulation system with zinc binding, the nonbond parameters of the Zn(II) used in this study were determined by modeling the active site of HCAII (human carbonic anhydrase II) using molecular orbital method by Hoops and co-workers.[49] By combining with the AMBER force field, this parameter set is widely used in simulating the conformational dynamics and binding thermodynamics of the zinc containing proteins. In this work, in addition to the above nonbond interactions, the distance constraints are added between the Zn(II) and its liganding atoms according to the experimental data, namely, the nitrogen atoms in the side chain of the Histidine residues (His6, His13 and His14) and the oxygen atom of the Glu11 carboxylate.[18] Such a strong bond interaction between the Zn(II) and the liganding atoms significantly weakens the dependence of the conformational distribution on the nonbond parameters.

The covalent bonds involving hydrogen atoms are constrained with the SHAKE algorithm, and the time step of 0.002 ps is used. Totally, 28 standard MD are run from $T = 283$ K to $T = 655$ K. The temperatures are selected with an exponential law which makes the acceptance ratio a constant. The time intervals between the exchange attempts are 0.8 ps, and the atomic coordinations are recorded every 0.4 ps for further analysis. Each replica is simulated for 70 ns, which results in the integration time of 1.96 μs. The configurations of the last 60 ns for each replica are used to extract the conformational distributions. In determining the structures of the most probable conformation, the cluster algorithm is used.[50] The PROSS protocol is used in assigning the secondary structures.[51]

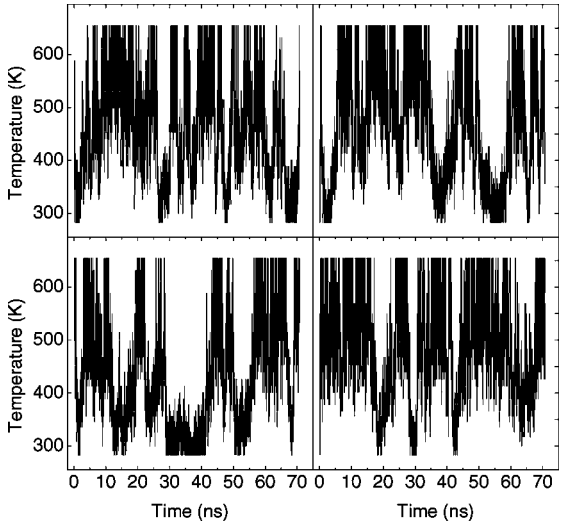

Figure 1. Temperature trajectories of four selected replicas.

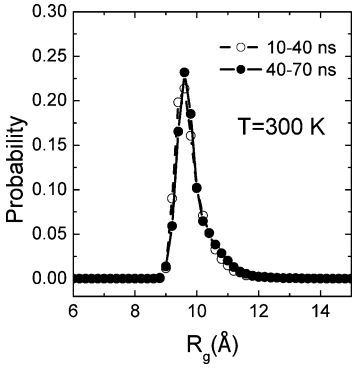

Figure 2. Distributions of the radius of gyration (R_g) for the conformations sampled during the time interval 10−40 ns (open circle and dashed line) and 40−70 ns (close circle and solid line).

It should be noted that the GB implicit solvent model used in this work may underestimate the importance of solvent screening in charge−charge interactions.[52] This effect can affect the secondary structure propensity of the peptide. Therefore, the absolute values of the calculated secondary structure probabilities may deviate from the real values. However, this shortcoming of the GB model can be largely eliminated in this work since we are just interested in the variation of the conformational distributions for the peptide with and without zinc binding. Such comparison dramatically reduces the influence of the systematic bias of the conformational distribution resulted from the implicit treatment of the solvent effect.

III. Results and Discussions

One of the advantages of the REMD is that it can give reproducible results in reasonable simulation time compared with the standard MD. Figure 1 shows the temperature trajectories for four selected replicas. One can see that a wide range of temperatures are visited by the replicas, illustrating high sampling quality. To further verify the convergence of the simulations, the distributions of the radius of gyration (R_g) for the conformations sampled during the time interval 10−40 ns and 40−70 ns are presented in Figure 2. One can observe that the distributions have no significant differences, which suggests that the sampling is well-converged. This means that we can

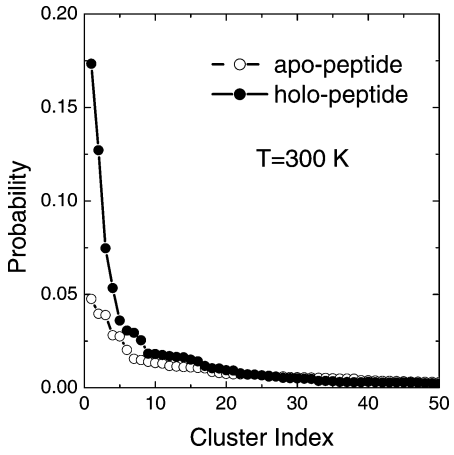

Figure 3. Percentages of the structures in each clusters of the holo-peptide (close circle and solid line) and the apo-peptide (open circle and dashed line) sampled at 300 K.

extract the effects of the zinc binding on the conformational distribution of the monomer and investigate the mechanism of the zinc induced conformational transition by directly comparing the conformational distributions of the Aβ peptides with and without zinc binding.

In order to investigate the difference of conformational distributions for the holo-peptide and the apo-peptide, we performed cluster analysis to the structures sampled by these two peptides at 300 K. Figure 3 gives the relative populations of each cluster for the holo-peptide (close circle with solid line) and apo-peptide (open circle with dashed line). The cutoff of the root mean square (rms) distance in assigning the clusters is 3.5 Å. One can find that the conformational distribution of the apo-peptide is more uniform compared with that of the holo-peptide. For example, the relative populations of the five most probable clusters for the holo-peptide are 17.3, 12.7, 7.5, 5.3, and 3.6%, respectively. In comparison, the relative populations of the five most probable clusters for the apo-peptide are 4.8, 4.0, 3.9, 2.8, and 2.8%, respectively. The small relative populations in the most probable clusters for the apo-peptide indicate that the structures of the apo-peptide are more heterogeneous than that of the holo-peptide. We also performed principal analysis to the structures sampled by these two peptides at 300 K. Figure 4 shows the free energy landscapes projected onto the first two principal components for the holo-peptide (a) and apo-peptide (b). One can see that the free energy landscapes are quite different for these two peptides. For example, the two most major states (dashed circles) for the holo-peptide are more dominantly populated compared with those of the apo-peptide. Such remarkable differences between the conformational distributions of the holo-peptide and those of the apo-peptide indicate that the zinc binding has significant influences on the conformational distribution of the Aβ monomer. Since the conformations of the Aβ monomer in solution may influence the pathogenic conformational transition during the peptide aggregation, the effect of the zinc binding on the conformational distribution of the monomer implies that the zinc binding could be involved in the conformational transition and aggregation of the Aβ peptide.

In Figure 5, we give the structures of the most probable clusters for the apo-peptide (a) and holo-peptide (b). One can see that, for the apo-peptide, the α-helix can be sampled for the segment 15−20. Meanwhile, the N-terminal segment 6−14 and the C-terminal segment 29−36 are tightly packed to each other. The segment 23−28 (the black region) is relatively extended. However, this segment forms a turn structure in the amyloid fibrils and plays a crucial role during the pathogenic folding of the Aβ monomer.[28,33−35] In comparison, in the most probable structure of the holo-peptide, there is no α helix being sampled. Meanwhile, the turn structure between the Asp23 and the Lys28 is largely formed. The segment 17−32 forms a hairpin-like structure with the segments 17−22 and 28−32 being the two strands. Such a structure is very similar to the strand−loop−strand structure observed by Han et al. with long-term molecular dynamics simulations of the Aβ_{10-35}.[25] The authors proposed that this strand−loop−strand structure could be the folding intermediate which contributes to the aggregation of the Aβ peptide. The higher probability for the holo-peptide to sample the 23−28 turn and the strand−loop−strand structure suggests that the zinc binding can promote the formation of the aggregation inclined monomer structures, which in turn contributes to the aggregation of the Aβ peptide.

In Figure 5, the formation probability of the central turn 23−28 is only qualitatively discussed. To further investigate the effect of the zinc binding on the formation of this central turn, we calculated the formation probability of the central turn for the apo-peptide and holo-peptide, and the results are presented in Figure 6. The results show that, at low temperature (<330 K), the zinc binding can increase the formation probability of the central turn. At higher temperatures, such effect vanishes. It is worth noting that in Figure 6, the formation probability of the central turn may be overestimated since the turn structures are assigned only on the basis of the dihedral angle of each

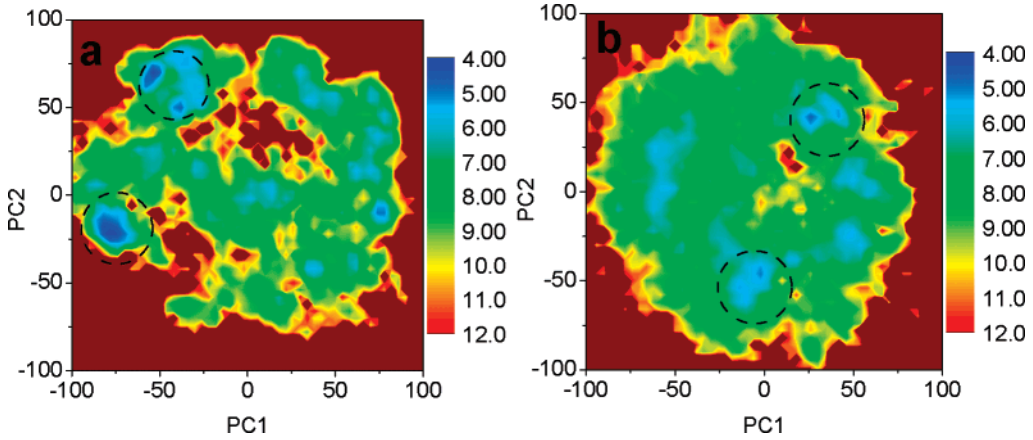

Figure 4. Free energy landscapes projected onto the first (PC1) and second (PC2) principal components for the holo-peptide (a) and apo-peptide (b) at 300 K. In this figure, the free energies are represented by $-k_BT$ lnP(PC1, PC2) with P(PC1, PC2) being the distribution probability calculated by the structures sampled at 300 K. The unit of the free energy is k_BT which T being the temperature, and k_B being the Boltzmann constant.

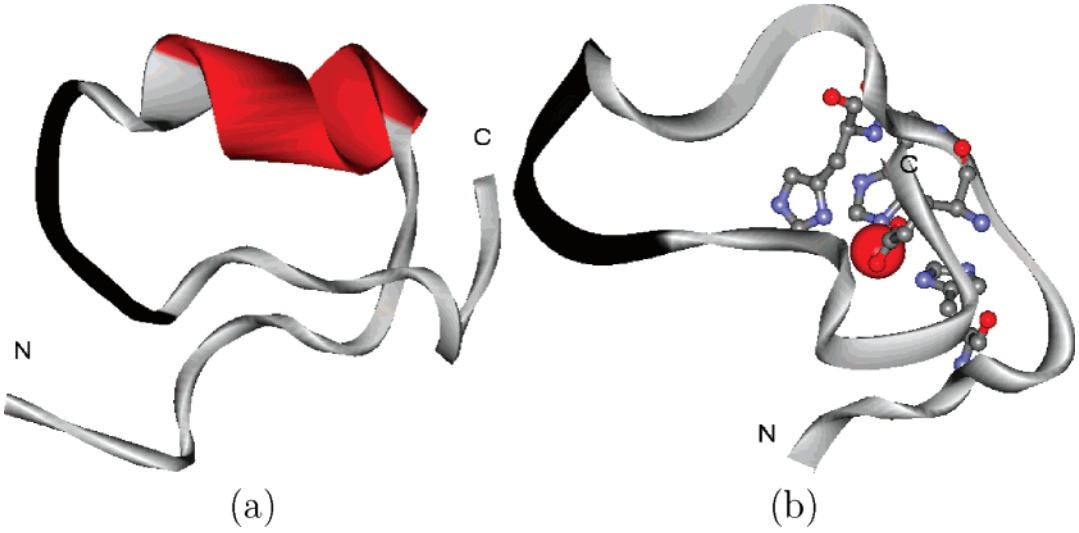

Figure 5. Structures of the most probable clusters for the apo-peptide (a) and holo-peptide (b) at 300 K.

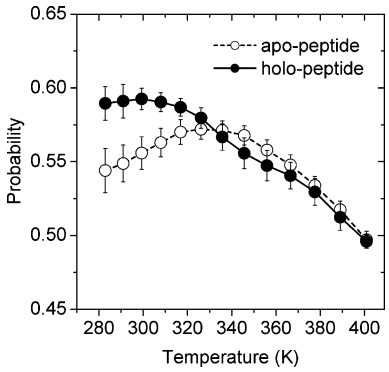

Figure 6. Averaged turn formation probabilities for the residues 23−28 as a function of temperature for the holo-peptide (close circle and solid line) and apo-peptide (open circle and dashed line). The assignment of the turn structure for each residue is based on the PROSS protocol. The error bars are calculated from the block average of 3 ns in length and represent the standard error.

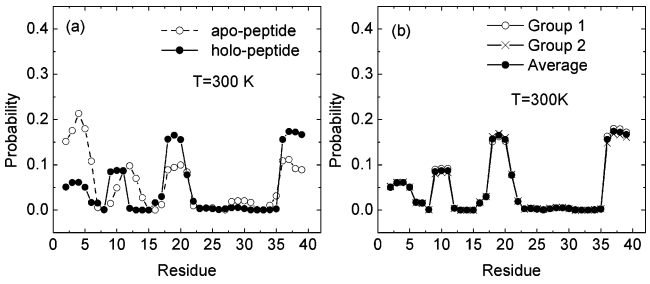

Figure 7. (a) Probability for each residues to sample the β-strand structure for the holo-peptide (close circle and solid line) and apo-peptide (open circle and dashed line) at 300 K. (b) Probability for each residues to sample the β-strand structure for the holo-peptide calculated from the structures of group 1 (open circle), group 2 (cross), and both (close circle) at 300 K. The structures are assigned to group 1 or group 2 alternately every 0.5ns.

residue in the 23−28 region using the PROSS protocol,[51] and the constraint of hydrogen bonds is not considered. However, we can still observe that the zinc binding can promote the turn formation by around 5% at room temperature, which can contribute to the aggregation of the Aβ peptide.

Solid-state NMR spectra suggested that the amyloid fibrils are dominated by parallel β-sheet structure.[7,53] However, in the aqueous and membrane mimicking environments, the Aβ mainly adopts α helix and random coil structures.[3−6] Therefore, formation of the amyloid fibril demands secondary structure conversion from the α helix and random coil to the β strand. To understand the role of the metal binding on the secondary structure conversion, we investigate the effects of the zinc binding on the β-strand propensity of the Aβ peptide. Figure 7a shows the probability of each residue sampling the β strand for the apo-peptide (open circle and dashed line) and holo-peptide (close circle and solid line), respectively. One can see that for both peptides, the hydrophobic cluster 17−21, the N-terminal segment, and the C-terminal segment have high probabilities to sample the β-strand structure. Particularly, one can observe that the zinc binding enhances the β-strand conformations of the hydrophobic cluster 17−21 significantly. A number of experiments suggested that this hydrophobic cluster, which has high β-strand propensity,[54] plays a crucial role in the aggregation of the Aβ peptide.[29−31] Meanwhile, solid-state NMR showed that this hydrophobic cluster adopts a β-strand structure in the amyloid fibrils.[53] It was also found that the shortened segment of the Aβ peptide comprising 16−22 can form fibrils with the strand organization.[55] These results imply that the β-strand conformation of this hydrophobic segment is critical for the aggregation of the Aβ peptide. The enhancement of the β-strand content of this segment by the zinc binding revealed in this work indicates that the zinc binding can contribute to the aggregation of the Aβ peptide by affecting the secondary structure distribution of the monomer. From Figure 7a, it is also observed that the zinc binding can increase the β-strand content of the C-terminal segment simultaneously. In comparison, the β-strand content of the N-terminal segment is decreased significantly.

To estimate the statistical error in Figure 7a, we divided the structures sampled by the holo-peptide at 300 K into group 1 and group 2 alternately every 0.5 ns. The probabilities for each residue to sample the β-strand structure for the holo-peptide calculated from the structures of group 1 (open circle), group 2 (cross), and both (close circle) at 300 K are presented in Figure 7b. One can see that there is little difference between these three groups, indicating that the statistic in Figure 7a is significant to extract the effect of zinc binding.

In vitro studies found that the formation of the amyloid fibril sensitively depends on the temperatures. Slightly elevated temperatures can enhance the amyloid fibril formation rate significantly. Therefore, it is important to explore the conformational distributions of the peptide at different temperatures and the effects of the zinc binding on the temperature depen-

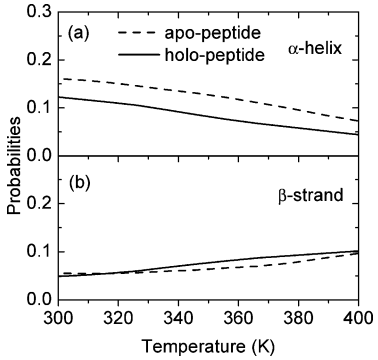

Figure 8. Averaged probabilities of the α helix (a) and the *β* strand (b) sampled by each residue in the holo-peptide (solid line) and the apo-peptide (dashed line) as a function of temperature.

dence. Figure 8 shows the averaged probabilities of the α helix (a) and the *β* strand (b) sampled by each residue in the apo-peptide (dashed line) and the holo-peptide (solid line) as a function of temperature. One can see that, with the increasing of the temperature, the α-helix content decreases rapidly, while the *β*-strand content increases slightly. These results suggest that slightly elevated temperatures can disrupt the α-helix structure, which in turn helps the peptide adopt a more extended *β* strand. This result is consistent with the experimentally observed acceleration of the aggregation process at slightly elevated temperatures. Compared with the apo-peptide, the holo-peptide samples less α-helical structures and slightly more *β*-strand structures. The less α-helical structures sampled by the holo-peptide may result from the geometric constraints imposed to the N-terminal segment. However, one can see from Figure 8b that the *β*-strand content for the holo-peptide is equal to or slightly higher than that for the apo-peptide, suggesting that the increasing of the *β*-strand propensity by the zinc binding for certain segments is accompanied by the decreasing of the *β*-strand content for the other segments. This result is consistent with the observation of Figure 7 which shows that the *β*-strand contents of the segment 17−21 and the C-terminal segment are increased significantly with the zinc binding, while that of the N-terminal segment is decreased largely. The counteraction between these two effects results in the overall enhancement being limited.

In both Figure 5a and Figure 8, the α-helical structures can be sampled by the peptide. However, there is no strong experimental evidence for the existence of helical structure for the A*β* monomer in the state simulated. Such high helical content observed in this work may be related to the force field used. In addition, the secondary structure assignment method used in this work may also overestimate the helical content since the secondary structure is assigned only on the basis of the dihedral angle of the main chain, and the constraint of the hydrogen bonds is not considered. However, the existence of helical structure in this simulation does not affect the conclusion of our work since we are only interested in the variation of the secondary structure contents with the binding of the metal ion but not the absolute secondary structure contents for each peptide.

It is worth noting that other simulations with explicit solvent in literature also observed helical structures.[26,27] Meanwhile, a recent experiment also gives signature that the α-helical content can be populated for the peptide with a similar condition.[54]

To further understand the effects of the zinc binding on the conformational distribution of the A*β* peptide, we constructed the contact maps for the A*β* peptides with and without zinc binding. Figure 9 shows the averaged contact maps for the holo-peptide (a) and apo-peptide (b) at 300 K. We define the contacts as occurring whenever two amino acid side chains, which separated by less than four amino acids, have any two heavy atoms within 5.0 Å. One can see that, compared with the apo-peptide, the holo-peptide has more long-range contacts which are mainly formed between the segment 28−40 and the segment 5−25. In comparison, the long-range contacts mainly formed between the segment 29−36 and the segment 6−14 for the apo-peptide, which is consistent with the structure of the largest cluster shown in Figure 5a. In the holo-peptide, because of the geometry constraints imposed by the zinc ion, the N-terminal segment has much higher contact probability.

From the solid-state NMR data of the amyloid fibrils, the backbone hydrogen bonds are mainly formed between the peptides and are responsible for the stabilization of the parallel *β* sheets.[7,53,56] In comparison, the intrapeptide interactions are dominated by the long-range side chain−side chain contacts (hydrophobic interaction, electrostatic interaction, and hydrogen bonds involving side chains). These long-range contacts not only define the interface of the *β* sheets, but also can contribute to the stabilization of the monomers within the fibril. The increasing of the long-range contacts by the zinc binding suggests that the intrapeptide interactions can be enhanced by the zinc binding, which may lead to the stabilization of the pathogenic monomer structure and contribute to the peptide aggregation. In particular, the contacts formed between the segment 28−40 and the segment 5−25 for the holo-peptide are helpful for the stabilization of the turn between Asp23 and Lys28 which is believed to be the folding nucleus for the pathogenic folding of the monomer during the A*β* aggregation.

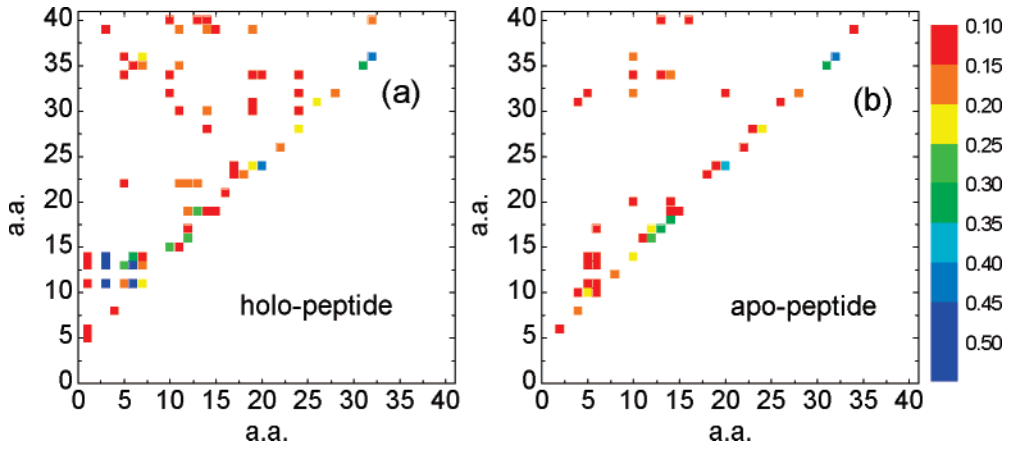

Figure 9. Averaged contact maps for the holo-peptide (a) and the apo-peptide (b) at 300 K.

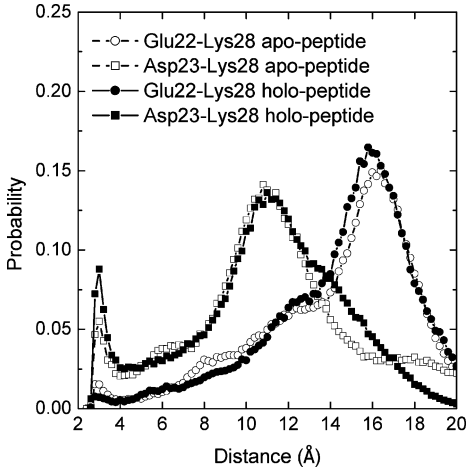

Figure 10. Distance distributions between the Asp23 and Lys28 (square) and between the Glu22 and Lys28 (circle) for the peptides with (close symbol and solid line) and without (open symbol and dashed line) zinc binding at 300 K. The distances between the anionic and the cationic residues are represented by the distances between the N of the NH_3 group and the O of the carboxylate.

It was found that the salt bridge between Asp23 and Lys28 is well-formed in the amyloid fibril. Experimental studies also showed that the preformation of the salt bridge between Asp23 and Lys28 can increase the Aβ_{1-40} fibrillogenesis rate by a factor of 1000.[32,28] Meanwhile, as the Asp23-Lys28 salt bridge locates at the ends of the central turn, formation of the salt bridge can contribute to the stabilization of this turn structure. Therefore, it is widely accepted that the formation of this salt bridge during the monomer folding is essential for the peptide aggregation.[19,28,32] Since the metal binding can dramatically influence the electrostatic interactions, we anticipate that the zinc binding can affect the formation of this salt bridge. Figure 10 shows the distance distributions between the Asp23 and Lys28. The distance distributions between the Asp22 and the Lys28 are also presented in the figure. One can see that, for both peptides, the distance between the Glu23 and Lys28 can vary within a wide range. At the distance of around 3.0 Å, there exists a sharp peak, which represents the formation of the Asp23−Lys28 salt bridge. We define the salt bridge formed whenever the distance between the N of the NH_3 group and the O of the carboxylate is less than 5.0 Å. With this definition, the formation probabilities of the Asp23−Lys28 salt bridges for the peptide with and without zinc binding are ∼7% and ∼10%, respectively. Therefore, this salt bridge only populated in a minority of structures for the Aβ monomer. There is no direct experimental measurement on the formation probability of the Asp23−Lys28 salt bridge in the Aβ monomer, whereas, among the 15 NMR structures of the Aβ_{10-35} deposited in the Protein Data Bank,[5] 6 of them form salt bridge according to the above-defined criterion, indicating that the Asp23−Lys28 salt bridge does not dominate the monomer structures of the Aβ peptide. Meanwhile, based on molecular dynamics simulations with CHARMM force field and explicit solvent, Thirumalai and co-workers investigated the formation of the Asp23−Lys28 salt bridge.[19] Consistent with our results, they found that the population of the Asp23−Lys28 salt bridge in the Aβ_{10-35} monomer is minor. On the basis of this observation, they proposed that the early stage of the Aβ oligomerization must involve the further formation of the Asp23−Lys28 salt bridge with the help of interpeptide interaction. However, the salt bridge formation probability obtained in the present work (∼10%) is lower compared with that of ref 19 (∼25%). This difference may be related to the differences of the force field and the length of the Aβ peptide (Aβ_{10-35} versus Aβ_{1-40}).

The most important result observed in this figure is that the holo-peptide has higher probability to form the Asp23−Lys28 salt bridge compared with the apo-peptide, which indicates that the zinc binding can promote the formation of the salt bridge Asp23−Lys28. In comparison, although the Glu22 is very close to the Asp23, the formation probability of the salt bridge Glu22−Lys28 is very low and is decreased by the zinc binding. Since the formation of the Asp23−Lys28 salt bridge can contribute to the amyloid fibril formation significantly, the enhancement of this salt bridge by the zinc binding suggests that the zinc binding can contribute to the Aβ aggregation by promoting the formation of the Asp23−Lys28 salt bridge. Assuming that the aggregation rate is proportional to the exponent of the concentration of the Aβ peptide with the Asp23−Lys28 salt bridge formed, the increase of the formation probability of the salt bridge (from ∼7% to ∼10%) by zinc binding can double the aggregation rate of the Aβ peptide, although the formation probability of this salt bridge is not predominant in the simulated monomer structures.

Previously, it was proposed that there exists competition between the carboxylate anions of the Glu22 and those of the Asp23 for the NH_3 group of the Lys28. The present results show that the salt bridge Asp23−Lys28 has a much higher formation probability compared with the salt bridge Glu22−Lys28, and the zinc binding can enhance this difference. Other simulations with discrete molecular dynamics also showed that, in conformations with a propensity for fibril formation, the electrostatic interactions between the Asp23 and the Lys28 are favored over those involving Glu22 and Lys28,[23] which is consistent with the above observations that the zinc binding can promote the formation of the aggregation inclined monomer conformations.

To understand the mechanism of the zinc binding enhanced formation of the salt bridge Asp23−Lys28, we explored the detailed interaction network between the anionic residues and the cationic residues. Figure 11 gives the salt bridge maps formed between all of the anionic and cationic residues of the Aβ peptides with (a) and without (b) zinc binding. One can see that the formation probabilities of the salt bridges are very different for these two peptides. Compared with the apo-peptide, the holo-peptide has a higher probability to form the salt bridge Asp23−Lys28, which is consistent with the observation of Figure 10. By comparing the salt bridge maps of the apo-peptide and the holo-peptide, one can observe that the salt bridges Glu3−Lys28 and Asp7−Lys28 are dramatically decreased because of the constraints imposed by the zinc binding, which makes the Asp23 and Lys28 have a higher probability to form a salt bridge.

In ref 19, Thirumalai and co-workers observed that the hydrogen bonds involving the discrete water molecules may affect the formation of the Asp23−lys28 salt bridge. However, because of the use of the implicit solvent model, such an effect cannot be captured in this work. Therefore, the absolute value of the formation probability for the Asp23−lys28 salt bridge may deviate from the real value.

It is interesting to note that Hummer and co-workers proposed that the charge−charge interactions between the intra- and the interpeptide Asp23−Lys28 in the manner of one-dimensional ionic crystalline interactions contribute to the stabilization of the fibril structure significantly.[57] The above results show that the zinc binding, by imposing geometric constraints to the N-terminal charged groups, decreases the charge−charge interactions between the N-terminal charged groups and the Lys28.

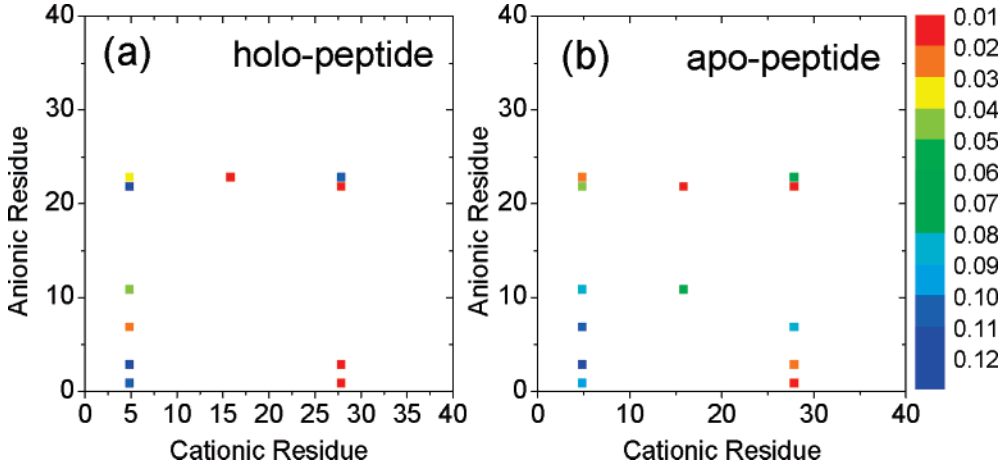

Figure 11. Salt bridge maps formed between all of the anionic and cationic residues of the Aβ peptide with (a) and without (b) zinc binding.

Such an effect can in turn increase the charge−charge interaction between the intra- and the interpeptide Asp23−Lys28. Therefore, the effect of the zinc binding on the salt bridge formation between the Asp23−Lys28 can also contribute to such one-dimensional ionic crystalline interactions as suggested by Hummer and co-workers, which is helpful for the formation and stabilization of the Aβ amyloid fibril.

In literature, two possible mechanisms are proposed for the metal promoted aggregation of the Aβ peptide: (I) the metal ion binds to two monomers simultaneously and contributes to the aggregation by bridging the peptides, and (II) each metal ion binds to one monomer and promotes the peptide to convert to a new conformation which is prone to aggregate. However, which mechanism is adopted by nature is still in debate. The present results demonstrate that the zinc binding can promote the formation of the aggregation inclined monomer structures of the Aβ peptide, which indicates that the metal ion induced conformation transition of the monomer is one of the possible mechanisms for the metal promoted aggregation of the Aβ peptide.

IV. Conclusions

In this work, we investigated the effects of metal binding on the conformational distribution of the full length Aβ peptide based on replica exchange molecular dynamics simulations. The results show that the zinc binding can affect the conformational distribution of the monomer dramatically. The peptide with zinc binding samples more conformations which is prone to aggregate compared with the peptide without zinc binding. Our results suggest that the metal induced conformational variation of the Aβ monomer is one of the possible mechanisms for the metal promoted aggregation of the Aβ peptide. The present work provides a deeper understanding to the metal dependent pathogenic folding and aggregation of the Aβ peptide which is essential for understanding the initial stage of the metal induced amyloid fibril formation.

Note that, in our simulations, the coordination bonds between the Zn(II) and the liganding atoms of the Aβ are preformed according to the NMR data. With this treatment, the convergence of the simulation can be better achieved, and we can investigate the effects of the zinc binding on the conformational distribution of the Aβ monomer. However, because of the preformation of the corresponding coordination bonds, the kinetic process of the zinc binding induced conformational transition cannot be described. To fully describe such effects, the whole binding process of the Zn(II) to the liganding atoms needs to be simulated. In addition, the present work only investigated the role of zinc binding on the conformational distribution of the Aβ monomer. To fully understand the zinc induced amyloid fibril formation, the aggregation of Aβ peptide involving Zn(II) needs to be simulated. These works are underway in our group.

Acknowledgment. The authors thank Shanghai Supercomputer Center for the computational support. This work was supported by the Foundation of NNSF (Nos. 1070433, 90403120, 10504012, 10474041, and 10774069) and National Basic Research Program of China (2006CB910302, 2007CB814806). J. Wang also thanks the support from FANEDD and NCET-05-0439.

References and Notes

(1) Selkoc, D. J. *Nature* **2003**, *426*, 900−904.
(2) Chiti, F.; Dobson, C. M. *Annu. Rev. Biochem.* **2006**, *75*, 333−366.
(3) Barrow, C. J.; Yasuda, A.; Kenny, P. T. M.; Zagorski, M. *J. Mol. Biol.* **1992**, *225*, 1075−1093.
(4) Shao, H. Y.; Jao, S. C.; Ma, K.; Zagorski, M. *J. Mol. Biol.* **1999**, *285*, 755−773.
(5) Zhang, S.; Iwata, K.; Lachenmann, M. J.; Peng, J. W.; Li, S.; Stimson, E. R.; Lu, Y.; Felix, A. M.; Maggio, J. E.; Lee, J. P. *J. Struct. Biol.* **2000**, *130*, 130−141.
(6) Coles, M.; Bicknell, W.; Watson, A. A.; Fairlie, D. P.; Craik, D. *Biochemistry* **1998**, *37*, 11064−11077.
(7) Benzinger, T. L. S.; Gregory, D. M.; Burkoth, T. S.; Miller-Auer, H.; Lynn, D. G.; Botto, R. E.; Meredith, S. C. *Proc. Natl. Acad. Sci. U.S.A.* **1998**, *95*, 13407−13412.
(8) Baumketner, A.; Shea, J. E. *J. Mol. Biol.* **2006**, *362*, 567−579.
(9) Adlard, P. A.; Bush, A. I. *J. Alzheimer's Disease* **2006**, *10*, 145−163.
(10) Lovell, M. A.; Robertson, J. D.; Teesdale, W. J.; Campbell, J. L.; Markesbery, W. R. *J. Neurol. Sci.* **1998**, *158*, 47−52.
(11) Cherny, R. A.; Legg, J. T.; McLean, C. A.; Fairlie, D. P.; Huang, X.; Atwood, C. S.; Beyreuther, K.; Tanzi, R. E.; Masters, C. L.; Bush, A. I. *J. Biol. Chem.* **1999**, *274*, 23223−23228.
(12) Bush, A. I.; Pettingell, W. H.; Multhaup, G.; Vonsattel, M. D.; Gusella, J. F.; Beyreuther, K.; Masters Tanzi, C. L. *Science* **1994**, *265*, 1464−1467.
(13) Atwood, C. S.; Moir, R. D.; Huang, X.; Scarpa, R. C.; Bacarra, N. M.; Romano, D. M.; Hartshorn, M. A.; Tanzi R. E.; Bush, A. I. *J. Biol. Chem.* **1998**, *273*, 12817−12826.
(14) Syme, C. D.; Nadal, R. C.; Rigby, S. E. J.; Viles, J. H. *J. Biol. Chem.* **2004**, *279*, 18169−18177.
(15) Miura, T.; Suzuki, K.; Kohata, N.; Takeuchi, H. *Biochemistry* **2000**, *39*, 7024−7031.
(16) Karr, J. W.; Akintoye, H.; Kaupp, L. J.; Szalai, V. A. *Biochemistry* **2005**, *44*, 5478−5487.
(17) Talmard, C.; Guilloreau, L.; Coppel, Y.; Mazarguil, H.; Faller, P. *Chem. Bio. Chem.* **2007**, *8*, 163−165.
(18) Zirah, S.; Kozin, S. A.; Mazur, A. K.; Blond, A.; Cheminant, M.; Segalas-Milazzo, I.; Debey, P.; Rebuffat, S. *J. Biol. Chem.* **2006**, *281*, 2151−2161.

(19) Tarus, B.; Straub, J. E.; Thirumalai, D. *J. Am. Chem. Soc.* **2006**, *128*, 16159−16168.
(20) Klimov, D. K.; Straub, J. E.; Thirumalai, D. *Proc. Natl. Acad. Sci. U.S.A.* **2004**, *101*, 14760−14765.
(21) Nguyen, P. H.; Li, M. S.; Stock, G.; Straub, J. E.; Thirumalai, D. *Proc. Natl. Acad. Sci. U.S.A.* **2007**, *104*, 111−117.
(22) Tarus, B.; Straub, J. E.; Thirumalai, D. *J. Mol. Biol.* **2005**, *345*, 1141−1156.
(23) Borreguero, J. M.; Urbanc, B.; Lazo Sergey, B.; Buldyrev, V.; Teplow, D. B.; Eugene Stanley H. *Proc. Natl. Acad. Sci. U.S.A.* **2005**, *102*, 6015−6020.
(24) Urbanc, B.; Cruz, L.; Yun, S.; Buldyrev, S. V.; Bitan, G.; Teplow, D. B.; Stanley, H. E. *Proc. Natl. Acad. Sci. U.S.A.* **2004**, *101*, 17345−17350.
(25) Han, W.; Wu, Y. D. *J. Am. Chem. Soc.* **2005**, *127*, 15408−15416.
(26) Flock, D.; Colacino, S.; Colombo, G.; Di Nola, A. *Proteins* **2006**, *62*, 183−192.
(27) Xu, Y.; Shen, J.; Luo, X.; Zhu, W.; Chen, K.; Ma, J.; Jiang, H. *Proc. Natl. Acad. Sci. U.S.A.* **2005**, *102*, 5403−5407.
(28) Lazo, N. D.; Grant, M. A.; Condron, M. C.; Rigby, A. C.; Teplow, D. B. *Protein Sci.* **2005**, *14*, 1581−1596.
(29) Miravalle, L.; Tokuda, T.; Chiarle, R.; Giaccone, G.; Bugiani, O.; Tagliavini, F.; Frangione, B.; Ghiso, J. *J. Biol. Chem.* **2000**, *275*, 27110−27116.
(30) Morimoto, A.; Irie, K.; Murakami, K.; Masuda, Y.; Ohigashi, H.; Nagao, M.; Fukuda, H.; Shimizu, T.; Shirasawa, T. *J. Biol. Chem.* **2004**, *279*, 52781−52788.
(31) Tjernberg, L. O.; Naslund, J.; Lindqvist, F.; Johansson, J.; Karlstrom, A. R.; Thyberg, J.; Terenius, L.; Nordstedt, C. *J. Biol. Chem.* **1996**, *271*, 8545−8548.
(32) Sciarretta, K. L.; Gordon, D. J.; Petkova, A. T.; Tycko, R.; Meredith, S. C.; *Biochemistry* **2005**, *44*, 6003−6014.
(33) Kirschner, D. A.; Inouye, H.; Duffy, L. K.; Sinclair, A.; Lind, M.; Selkoe, D. J. *Proc. Natl. Acad. Sci. U.S.A.* **1987**, *84*, 6953−6957.
(34) Barrow, C. J.; Zagorski, M. G. *Science* **1991**, *253*, 179−182.
(35) Straub, J. E.; Guevara, J.; Huo, S.; Lee, J. P. *Acc. Chem. Res.* **2002**, *35*, 473−481.
(36) Sugita, Y.; Okamoto, Y. *Chem. Phys. Lett.* **1999**, *314*, 141−151.
(37) García, A. E.; Sanbonmatsu, K. Y. *Proteins* **2001**, *42*, 345−354.
(38) García, A. E.; Onuchic, J. N. *Proc. Natl. Acad. Sci. U.S.A.* **2003**, *100*, 13898−13903.
(39) Zhou, R.; Berne, B. J.; Germain, R.; *Proc. Natl. Acad. Sci. U.S.A.* **2001**, *98*, 14931−14936.
(40) Zhang, J.; Qin, M.; Wang, W. *Proteins* **2006**, *62*, 672−685.
(41) Li, W.; Zhang, J.; Wang, W. *Proteins* **2007**, *67*, 338−349.
(42) Felts, A. K.; Narano, Y.; Gallicchio, E.; Levy, R. M. *Proteins* **2004**, *56*, 310−321.
(43) Nguyen, P. H.; Stock, G.; Mittag, E.; Hu, C. K.; Li, M. S. *Proteins* **2005**, *61*, 795−808.
(44) Cecchini, M.; Rao, F.; Seeber, M.; Caflisch, A. *J. Chem. Phys.* **2004**, *121*, 10748−10756.
(45) Zhou, R. *J. Mol. Graph. Model.* **2004**, *22*, 451−463.
(46) Case, D. A.; Darden, T. A.; Cheatham, T. E., III; Simmerling, C. L.; Wang, J.; Duke, R. E.; Luo, R.; Merz, K. M.; Wang, B.; Pearlman, D. A.; Crowley, M.; Brozell, S.; Tui, V.; Gohlke, H; Mongan, J.; Hornak, V.; Cui, G.; Beroza, P.; Schafmeister, C.; Caldwell, J. W.; Ross, W. S.; Kollman, P. A. AMBER 8, University of California: San Francisco, CA, 2004.
(47) Duan, Y.; Wu, C.; Chowdhury, S.; Lee, M. C.; Xiong, G.; Zhang, W.; Yang, R.; Cieplak, P.; Luo, R.; Lee, T.; Caldwell, J.; Wang, J.; Kollman, P. A. *J. Comp. Chem.* **2003**, *24*, 1999−2012.
(48) Onufriev, A.; Bashford, D.; Case, D. A. *J. Phys. Chem. B* **2000**, *104*, 3712−3720.
(49) Hoops, S. C.; Anderson, K. W.; Merz, K. M., Jr. *J. Am. Chem. Soc.* **1991**, *113*, 8262−8270.
(50) Snow, C. D.; Qiu, L.; Du, D.; Gai, F.; Hagen, S. J.; Pande, V. S. *Proc. Natl. Acad. Sci. U.S.A.* **2004**, *101*, 4077−4082.
(51) Srinivasan, R.; Rose, G. D. *Proc. Natl. Acad. Sci. U.S.A.* **1999**, *96*, 14258−14263.
(52) Zhou, R.; Berne, B. J. *Proc. Natl. Acad. Sci. U.S.A.* **2002**, *99*, 12777−12782.
(53) Tycko, R. *Biochemistry* **2002**, *42*, 3151−3159.
(54) Hou, L.; Shao, H.; Zhang, Y.; Li, H.; Menon, N. K.; Neuhaus, E. B.; Brewer, J. M.; Byeon, I.-J. L.; Ray, D. G.; Vitek, M. P.; Iwashita, T.; Makula, R. A.; Przybyla, A. B.; Zagorski, M. G *J. Am. Chem. Soc.* **2004**, *126*, 1992−2005.
(55) Balbach, J. J.; Ishii, Y.; Antzutkin, O. N.; Leapman, R. D.; Rizzo, N. W.; Dyda, F.; Reed, J.; Tycko, R. *Biochemistry* **2000**, *39*, 13748−13759.
(56) Ferguson, N.; Becker, J.; Tidow, H.; Tremmel, S.; Sharpe, T. D.; Krause, G.; Flinders, J; Petrovich, M.; Berriman, J.; Oschkinat, H.; Fersht, A. R. *Proc. Natl. Acad. Sci. U.S.A.* **2006**, *103*, 16248−16253.
(57) Buchete, N.-V.; Tycko, R.; Hummer, G. *J. Mol. Biol.* **2005**, *353*, 804−821.